GDCh Research Article Angewandte International Edition Chemie www.angewandte.org

How to cite: *Angew. Chem. Int. Ed.* **2025**, *64*, e202505811
doi.org/10.1002/anie.202505811

High-Pressure Chemistry

Synthesis of Gold Hydride at High Pressure and High Temperature

Mungo Frost, Kilian Abraham, Alexander F. Goncharov, R. Stewart McWilliams, Rachel J. Husband, Michal Andrzejewski, Karen Appel, Carsten Baehtz, Armin Bergermann, Danielle Brown, Elena Bykova, Anna Celeste, Eric Edmund, Nicholas J. Hartley, Konstantin Glazyrin, Heinz Graafsma, Nicolas Jaisle, Zuzana Konôpková, Torsten Laurus, Yu Lin, Bernhard Massani, Maximilian Schörner, Maximilian Schulze, Cornelius Strohm, Minxue Tang, Zena Younes, Gerd Steinle-Neumann, Ronald Redmer, and Siegfried H. Glenzer*

Abstract: Gold is an unreactive metal and its chemical interactions with hydrogen have only recently been explored. Here, we report the formation of gold hydride above 40 GPa and 2200 K in X-ray free electron laser heated diamond anvil cells using various hydrocarbons as hydrogen sources. Above 40 GPa, a hexagonal phase emerges close to the gold melting point, corresponding to a hydride with stoichiometry Au_2H_x, with x increasing from 0 to near 1 with pressure from 40 to 80 GPa. This is a high-temperature phase which reverts to face centered cubic gold on cooling to 295 K. Accompanying DFT-MD simulations are in excellent agreement with experiment and reveal the structure to consist of an hexagonal close packed gold lattice with atomic hydrogen disordered in the interstices. The hydrogen is superionic and exhibits high diffusivity through the crystalline gold lattice. Our results present the first solid-state binary compound of gold and hydrogen.

Introduction

Gold is one of the least reactive metals and its chemistry, in particular its interactions with hydrogen, has only been explored recently.[1,2] Much of the work had been performed in the gas phase or at liquid helium temperatures, although recent developments in organometallic chemistry have led to the successful synthesis of hydrogen complexes,[3] and complexes of gold with hydrogen ligands.[2,4,5] In the gas phase, gold hydride and gold deuteride species have been inferred from UV absorption spectra[6] and photoelectron spectroscopy.[7] Cryogenic studies have reacted laser ablated gold with hydrogen and excess inert gas which was then condensed at 3.5 K.[8,9] This results in the formation of isolated AuH, AuH_2, $(H_2)AuH$, and the ions AuH_2^- and AuH_4^-, all of which decompose on warming.

The gold–hydrogen bond has an unusually covalent nature for a metal–hydrogen interaction owing to the high electronegativity of gold, which arises from relativistic effects.[10] On the Pauling scale, the electronegativity of gold is 2.54, which is higher than that of hydrogen, 2.2, with the result that the Au—H bond is expected to have a negatively polarized gold atom. This motivated studies which have demonstrated Au as a hydrogen bond acceptor.[1,11–13] Hydrogen–gold interactions are of interest in the field of catalysis, where heterogeneous gold nanoparticles exhibit excellent selectivity

[*] M. Frost, D. Brown, N. J. Hartley, S. H. Glenzer
High Energy Density Sciences Division, SLAC National Accelerator Laboratory, 2575 Sand Hill Road, Menlo Park, CA 94025, USA
E-mail: mdfrost@slac.stanford.edu

K. Abraham, A. Bergermann, M. Schörner, R. Redmer
Institut für Physik, Universität Rostock 18051, Rostock, Germany

A. F. Goncharov, E. Edmund
Earth and Planets Laboratory, Carnegie Institution for Science, 5241 Broad Branch Rd., NW, Washington, DC 20015, USA

R. S. McWilliams, N. Jaisle, B. Massani, Z. Younes
Centre for Science at Extreme Conditions and School of Physics and Astronomy, University of Edinburgh, King's Buildings, Edinburgh EH9 3FD, UK

R. J. Husband, K. Glazyrin, H. Graafsma, T. Laurus, C. Strohm
Deutsches Elektronen-Synchrotron DESY, Notkestr. 85 22607, Hamburg, Germany

M. Andrzejewski, K. Appel, Z. Konôpková, M. Tang
High Energy Density Scientific Instrument, European XFEL, Holzkoppel 4, Schenefeld 22869, Germany

C. Baehtz
Helmholtz-Zentrum Dresden-Rossendorf eV 01328, Dresden, Germany

E. Bykova
Institute of Geosciences, Goethe University Frankfurt 60438, Frankfurt, Germany

A. Celeste
Department of Earth and Planetary Science, Stanford University, 367 Panama Street, Stanford, CA 94305, USA

Y. Lin
Stanford Institute for Materials and Energy Sciences, SLAC National Accelerator Laboratory, 2575 Sand Hill Road, Menlo Park, CA 94025, USA

M. Schulze, G. Steinle-Neumann
Bayerisches Geoinstitut, Universität Bayreuth 95440, Bayreuth, Germany

Additional supporting information can be found online in the Supporting Information section

for certain hydrogenation reactions.[14] Hydrogen has further been observed to bond with gold nanoclusters due to the enhanced reactivity of the surface electronic states.[15,16]

There has been a similar degree of interest in gold hydrides in the solid state. Gold forms no binary hydrides at ambient pressure, but the widespread nature of transition metal hydrides under pressure has prompted studies of the gold–hydrogen system under pressure, as the hydrogen affinity of most metals greatly increases. This can cause metals which do not form hydrides at ambient pressure to adopt novel high-pressure compounds with hydrogen,[17–19] and greatly increase the hydrogen content of others.[20–22] High pressure hydrides are of interest of various fields including hydrogen storage[23] and high-temperature superconductivity.[21,22] However, a solid-state binary hydride of gold has remained elusive, with a few publications reporting its absence at high pressure,[24–26] and likely many more failed attempts which have gone unreported.

Hydrogen is challenging to contain at high pressure due to its reactions with pressure cell components and high mobility within many materials resulting in its loss from the sample environment.[27] Owing to its supposed non-hydride forming nature, gold coatings are widely used as a hydrogen permeation barrier in the study of high-pressure hydrogen,[28–31] offering further indication that the low hydrogen solubility in gold observed near ambient conditions[32] persists to megabar pressures.

Theoretical studies of the gold–hydrogen system have found no stable binary hydrides,[24,26] but the addition of alkali metals has been suggested for the synthesis of a stable ternary hydride.[24] Only two ternary gold-metal-hydrides are experimentally known: Nb_3AuH_x and Ti_3AuH_x, with $1 < x < 4.2$. Both have cubic A15 structures, but gold is the minority species with another hydride forming metal.[33,34]

Here we report the X-ray free electron laser (XFEL) synthesis of a hexagonal gold hydride with stoichiometry Au_2H_x, with $x < 1$, above ~2200 K and 40 GPa. XFEL pump-probe measurements indicate that it adopts a hexagonal structure, reminiscent of that of Cu_2H,[25] with a hexagonal close packed (*hcp*) Au lattice, but decomposes on cooling to ambient temperature, where face centered cubic (*fcc*) gold is recovered with no evidence of dissolved hydrogen. Density functional theory molecular dynamics (DFT-MD) calculations support the structural assignment and indicate that hydrogen is superionic in the lattice. This result highlights the importance of studying novel extreme conditions chemistry and properties at high-pressure and high-temperature conditions, rather than considering only samples quenched back to ambient temperature.

Results and Discussion

The samples consisted of gold embedded in various hydrocarbons compressed in diamond anvil cells (DACs). The hydrocarbon served as insulation for the anvils, the pressure transmitting medium, and the hydrogen source, as hydrogen is produced by the precipitation of the carbon as diamond or graphite depending on pressure.[35–37] Methane (CH_4), polyethylene ($(CH_2)_n$), polystyrene ($(C_8H_8)_n$) and coronene ($C_{24}H_{12}$) were used.

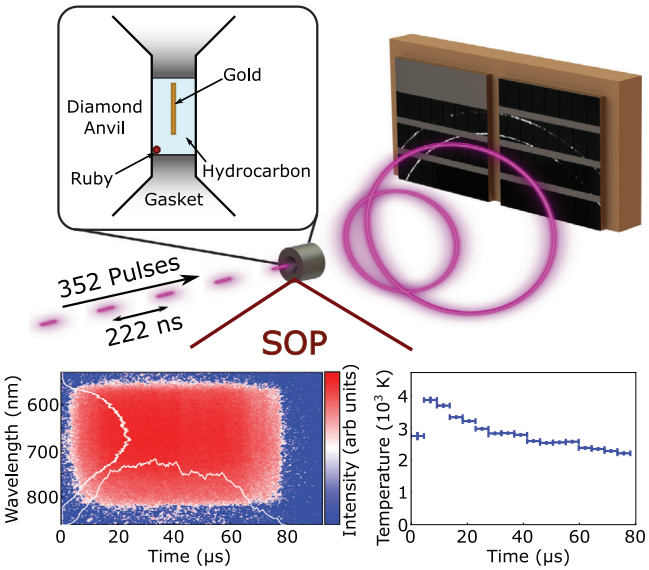

Figure 1. Setup of the XFEL experiment: 352 X-ray pulses from the XFEL are incident on the sample at 4.5 MHz (center), with diffraction recorded on the large area AGIPD detector (upper right). The left upper panel shows the sample configuration with perforated gold foil embedded in a hydrocarbon and compressed between diamond anvils. The lower panels show the streaked optical pyrometry data, with a raw spectrogram on the left, where red corresponds to a stronger signal; white lines are the intensity vs. wavelength averaged over time and total intensity vs. time. Temperature extracted from the spectrogram on the left via fitting to a Planck function is shown on the right.

Gold was heated and probed using high-intensity X-rays at the European XFEL. X-ray pulses of < 50 fs duration were incident on the gold sample in pulse trains with a frequency of 4.5 MHz. The transit of each X-ray pulse through the sample results in the deposition of heat into the sample, as well as the collection of an X-ray diffraction (XRD) pattern. The XFEL pulse duration is shorter than the timescale of nuclear motion,[38,39] so the diffraction occurs before the lattice response and the XRD probes the structure of the sample at the maximal cooling time, 222 ns after the previous pulse. The time-resolved temperature was measured using streaked optical pyrometry (SOP).[36,38] A diagram of the experimental setup is shown in Figure 1, with full experimental details given in the Supporting Information.

Up to 39 GPa initial pressure, no reaction between hydrocarbons and gold is observed, though diamond is observed to precipitate in agreement with previous results,[36] implying that there is an excess hydrogen-rich phase remaining. At, and above, a starting pressure of 41 GPa, new peaks with a strikingly different texture from *fcc* gold emerge in the diffraction pattern as shown in Figures 2 and 3. Diffraction patterns with the new phase present always also show an increased background signal attributed to liquid diffuse scattering from molten gold, as well as residual *fcc* gold. The appearance of the new phase in the presence of liquid diffuse scattering suggests that it occurs at high temperatures close to the melting point of gold. This diffuse scattering is subtracted

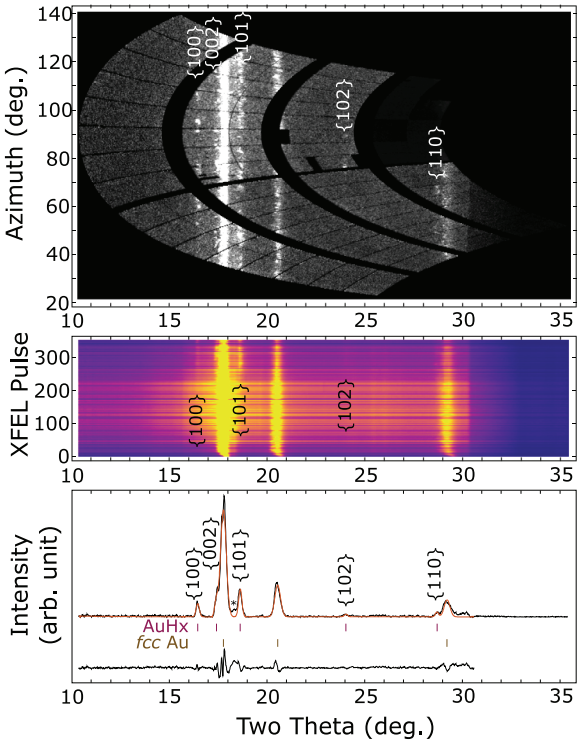

Figure 2. AGIPD diffraction image sequence from a run of gold in coronene starting at 56 GPa, $\lambda = 0.6888$ Å. Hydride peaks are marked with {*hkl*}. Top: an azimuthally unwrapped ("caked") image from the AGIPD detector. The image is the final pulse (number 352) from the middle panel. Diffraction from the hydride is primarily in isolated spots differentiating it from the residual *fcc* gold and indicating a few larger crystallites rather than fine powder. Middle: Background-subtracted integrated diffraction patterns from each pulse of the run with intensity normalized to account for jitter in the pulse energies showing the hydride to form around after pulse 200. Bottom: LeBail fit to the background-subtracted integrated pattern of the final pulse showing the *hcp* hydride with residual *fcc* gold. Data is in black, fit in orange and residual is lower black trace. Ticks indicate allowed peak positions. Data above 31° are not fitted as the diamond anvil cell shadowed higher angles. The asterisk indicates a peak from the tungsten gasket. Similar data from other runs are shown in Figures S2 and S3.

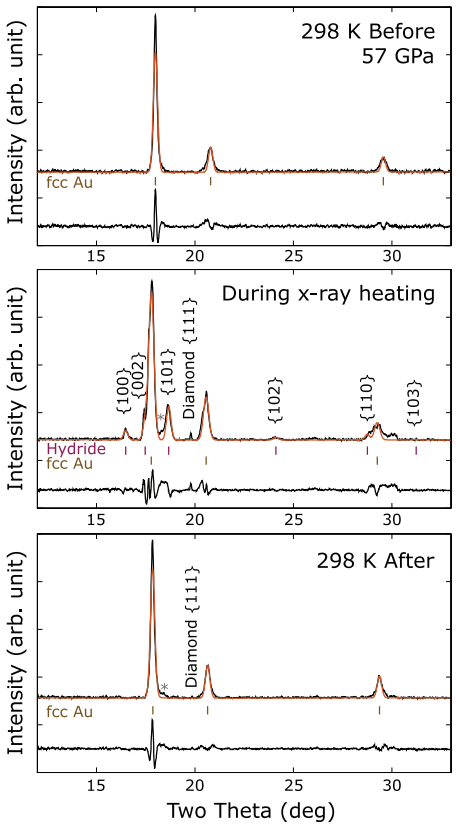

Figure 3. Background-subtracted integrated powder X-ray diffraction before (top), during (middle) and after (bottom) heating of gold embedded in coronene at 57 GPa. The upper black lines show the data with a LeBail fit in orange, the lower black line is the residual. The new peaks occur only at high temperature and correspond to a hexagonal close packed structure with peaks labeled. The {100}, {101}, and {102} peaks are well resolved, while the {002} and {110} peaks partially overlap with *fcc* gold peaks. Pyrometry (Figure 1) gives $T = 3500(500)$ K; however, the presence of solid *fcc* gold implies strong thermal gradients such that the sample is partially below the melting point of gold. Patterns are from single XFEL pulses of $\lambda = 0.6888$ Å, the "before" and "after" patterns were taken with a highly attenuated beam to avoid heating. The diamond formed by loss of hydrogen from the coronene is detectable during and after heating. The peak marked with an asterisk during heating is from the tungsten gasket.

with the background when fitting crystalline phases, but is shown in Figure S1. The presence of *fcc* gold is attributed to temperature gradients in the probed area.[40]

The new peaks are of higher intensity than could arise from the low Z hydrogen or carbon, and are of similar intensity to those of the remaining *fcc* gold, implying that they must arise from a phase containing the much more strongly scattering gold. They can be indexed to an *hcp* structure. In all cases the hexagonal {100} and {101} peaks of the emergent phase are clearly observed, allowing both *a* and *c* to be fitted reliably, giving c/a ratios close to ideal. In many cases other peaks are also resolvable as shown in the integrated powder X-ray diffraction patterns in Figure 3 and Figures S2 and S3. The *hcp* {002} peak overlaps with the {111} peak of the residual *fcc* gold, but has a different texture in the diffraction images consisting of isolated spots rather than lines, see Figure 2. This is indicative of fewer larger crystallites forming compared to the powder rings of the unreacted *fcc* gold. The reduced powder statistics results in variable peak intensities for the *hcp* gold hydride based on the orientations at which the crystals form with the result that higher order peaks only appear in some patterns.

The peaks arising from the new phase appear and persist only at high temperature and are absent in the quenched sample, implying that it is only stable at high temperature. After cooling, only peaks from *fcc* gold and diamond formed by precipitation from the hot hydrocarbon[36] are observed as shown in Figure 3. Diffraction maps of a cell after XFEL exposure at the PETRA-III synchrotron source (beamline P02.2), which offers higher *q* resolution and smaller probe beam than the XFEL, revealed only *fcc* gold with no residual *hcp* phase. Raman spectra taken after the XFEL experiment in a sample where gold hydride was synthesized from methane indicate that on decomposition gold hydride forms molecular

hydrogen in addition to *fcc* gold. H_2 is observed in the form of $(CH_4)_2H_2$.[41] Figure S4 shows the H_2 Raman stretching feature, demonstrating the presence of excess hydrogen from the decomposition of the hydrocarbon and hydride.

The *hcp* peaks which emerge at high temperature are narrower than those of the unreacted *fcc* gold, see Figures 2 and 3. This is due to thermal gradients in the gold coupler and is also observed in other XFEL pump-probe experiments.[36,42] The XFEL beam has a wider low intensity region surrounding the central high intensity focus which causes negligible heating, but does contribute signal from unheated gold on the detector, while near the beam center the gold is molten, see Figure S1. Thus the *fcc* gold peaks have contributions from gold at temperatures spanning from near ambient to the melting point, ~ 2500 K.[43] The *hcp* gold hydride is only stable at high temperature and is therefore subject to smaller thermal gradients. Additionally, it undergoes recrystallization on formation, as indicated by the distinct texture of the hydride diffraction, shown in Figure 2. This will relax nonhydrostatic strain and remove strain broadening in the hydride which might be present in the unreacted *fcc* gold.

Unit cell volumes fitted for many runs in different samples are shown in Figure 4, with the individual cell parameters and c/a ratio in Figure S5. The volume per gold atom of the fitted *hcp* unit cell is larger than that of *fcc* gold at the same pressure. The *hcp* structure does not occur in pure gold at this pressure, which suggests the formation of gold hydride, with the hydrogen accounting for the excess volume. Copper, another group 11 element, is known the form a hexagonal Cu_2H hydride with $P\bar{3}m1$ symmetry (anti-CdI_2-type structure) at 18.6 GPa,[25] in which hydrogen atoms occupy alternate inter-layers. This has a c/a ratio of 1.66, similar to the values obtained for the novel gold compound which is generally between 1.65 and 1.7. The measured volume shows variation at a given pressure, independent of the hydrocarbon used as a hydrogen source material. This variation is larger than can be attributed to fit uncertainty and is likely due to a combination of temperature and pressure variations and reaction rate limitations,[36] leading to variable stoichiometry of the hydride.

The structure of the hexagonal gold hydride was explored using DFT-MD, starting with Au_2H in the Cu_2H structure, and successively and randomly removing hydrogen atoms to create H-deficient structures, which produced unit cell volumes similar to those observed experimentally. The simulations were conducted at 2500 K and pressures covering the range of experimental observations, as shown in Figures 4 and S7. For all compositions, we find the hydrogen atoms to be highly mobile in the lattice, and they rapidly ($\lesssim 0.2$ ps) equilibrate to occupy the interstices in all layers equally. While there are significant dynamics in the gold lattice, it overwhelmingly retains the *hcp* structure as revealed by a Voronoi cell topology analysis[44,45] as shown in Figure S8. While the c/a ratio in the hexagonal structure cannot be directly extracted from simulations, the anisotropic stress is reduced for ratios slightly above ideal, see Figure S6, in agreement with experimental data, see Figure S5.

The novel phase is assigned to be a hydride rather than a carbide or novel phase of pure gold, for several reasons. First,

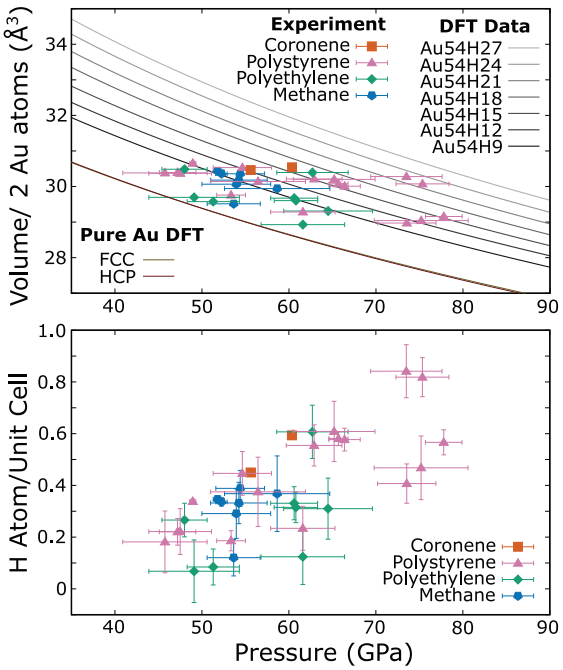

Figure 4. The pressure dependence of the experimentally measured volumes of gold hydride imply increasing hydrogen content with pressure. Top: Volume per two gold atoms from experiment and DFT-MD results at 2500 K. Curves are 2nd-order Birch–Murnaghan fits to DFT-MD results, the shades of gray correspond to different concentrations of hydrogen (number of atoms in the $3 \times 3 \times 3$ supercell with 54 gold atoms, $Au_{54}H_x$). DFT-MD volumes of pure Au at 2500 K with *fcc* (gold) and *hcp* (dark red) structures are virtually indistinguishable. Points show experimental data colored by precursor hydrocarbon, error bars cover the possible bounds on pressure during heating, as discussed in the Supporting Information. Bottom: Hydrogen content per *hcp* unit cell in the experiments based on the hydrogen excess volumes from DFT-MD. The *hcp* {100} and {101} peaks were used for fitting as other peaks are not always well resolved. Error bars correspond to plausible pressure range and variation in H content based on that pressure range.

its volume is higher than expected for pure gold implying an additional constituent, see Figure 4. Second, other XFEL pump-probe experiments which used gold couplers to heat water using a similar sample geometry did not form *hcp* gold at similar conditions.[42] This implies that the hydrocarbon is involved in the formation of the *hcp* phase. Hydrogen is much more strongly bound in water than in hydrocarbons,[46] and dehydrogenation of hydrocarbons by metals is well known even at ambient temperature and mild pressure.[47–49] Third, under the conditions studied, carbon is precipitated from the hot hydrogen–carbon mixture as diamond which can be detected in the powder X-ray diffraction pattern shown in Figure 3, leaving excess hydrogen. Fourth, the formation of gold carbide is improbable as there is insufficient excess volume, and no reaction with the carbon from the diamond anvils has been observed in gold heated in DACs.[38,42,43]

As well as supporting the experimentally proposed structure, the calculations can offer additional insight into the gold hydride phase. Simulations on pure gold at 2500 K in the same pressure range with *fcc* and, theoretical, *hcp* structures find their volumes to be very similar. Consideration of the excess

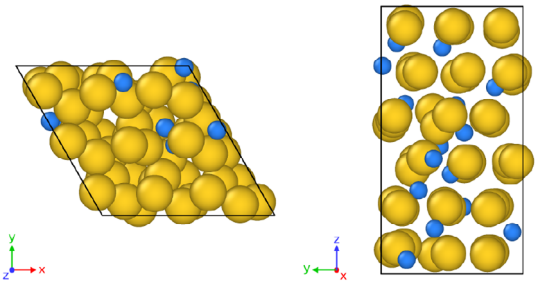

Figure 5. Snapshot from the molecular dynamics simulations for $Au_{54}H_{15}$ (3 x 3 x 3 supercell) at ~ 65 GPa and 2500 K, with Au atoms in gold and H atoms in blue. The boundaries of the hexagonal cell are shown by black lines, with supercell constants of $a = b = 8.305$ Å and $c = 13.561$ Å. The structure is projected down the *c*-axis (left) and the *a*-axis (right).

volume of the DFT-MD simulated gold hydrides over pure *hcp* gold allows for an estimate of the hydrogen content of the experimentally observed gold hydride, as shown in Figure 4. Comparison of the unit cell volumes for gold hydrides of varying hydrogen content and hydrogen-free gold simulated in an *hcp* lattice reveals that the volume per hydrogen atom decreases with pressure but is insensitive to composition, as illustrated in Figure S9, showing that the linear mixing approximation holds in this regime. Comparison to the experimentally fitted volumes reveal the gold hydride to be hydrogen-poor with stoichiometry Au_2H_x with x increasing from close to 0 at 40 GPa to almost 1 by 80 GPa, see Figure 4. On removing hydrogen from the lattice, no ordering is observed in the vacancies.

The DFT-MD simulations ran for up to 15 ps for a few cases which allowed the trajectories of the ions to be investigated as a function of time. They reveal the hydrogen atoms to be superionic in the *hcp* gold lattice, exhibiting rapid diffusion through it. The mean squared displacements of both atom types as a function of time are shown in Figure S10 for $Au_{54}H_{15}$ at ~ 65 GPa and 2500 K (sample configuration during the simulation shown in Figure 5). Gold atoms remain bound to their lattice sites with low diffusivity, but hydrogens diffuse rapidly, with values of $D = 3.0(0.9) \times 10^{-6}$ cm^2 s^{-1} and $D = 5.9(0.9) \times 10^{-4}$ cm^2 s^{-1}, respectively. Given the virtually constant atomic volume of hydrogen in the hydride structure with composition, see Figure S9, alterations to hydrogen–hydrogen interactions are likely to be limited and diffusion constants do not differ significantly at a given pressure. However, there is a general trend of decreasing diffusivities, within a factor of $2-3$, for the pressure range considered $(40-80$ GPa).

Recent years have seen considerable development in gold chemistry, and particularly chemical interactions between hydrogen and gold. The unexpected reactivity of gold at combined high-pressure and high-temperature conditions implies that the general inertness of gold does not hold under extreme conditions, where it exhibits enhanced reactivity. How broadly this is applicable to other noble metals, or chemistry in general is yet to be determined. The gold hydride reported here is the first observed binary solid state compound of gold and hydrogen. It forms at pressure above 40 GPa and near the melting point of gold, ~2500 K.[43] On cooling at high pressure, the hydride decomposes recovering *fcc* gold. Gold chemistry at extreme conditions impacts high-pressure experiment where gold is widely assumed to be an inert sample component used for determining pressure, sample containment and as a coupler for heating DACs.[31,36,50] The results here, shown in Figure S11, show that care must be taken in extrapolation of existing thermal equations of state to temperatures near the melting point and that unexpected chemistry at extreme conditions must be considered in designing such experiments.

The unexpected reactivity of gold and hydrogen serves as another example of unusual chemistry occurring at extreme pressures. The field of extreme conditions chemistry has seen many surprising developments in recent years, such as alkali metal polyhalides,[51,52] unusual structures of the higher metal nitrides,[53–55] and XFEL induced chemistry in yttrium hydride.[56] The opening of novel chemistry by pressure arises from the pressure–volume contribution to the free energy approaching, or even exceeding, that of the chemical bonds with the result that energetically less favorable bonding schemes may become thermodynamically stable if they allow for sufficiently increased density.[57] Most previous studies of extreme conditions chemistry have investigated quenched samples. The discovery of a compound which is stable only at combined high-pressure and high-temperature suggests a new avenue of extreme conditions chemical interactions which can only be explored in situ.

Our calculations find that the hydrogen ions are superionic in the gold hydride presented here. Superionicity has been reported in some high-pressure hydrides with high hydrogen:metal ratios,[58–62] but is less known in binary metal-rich hydrides such as the gold hydride reported here.[63] For example, LaH_{10} is predicted to exhibit superionicy in the hydrogen at 170 GPa and 1500 K, albeit with less than a third of the hydrogen diffusivity reported here.[64] Iron hydride has also been predicted to become superionic at extreme conditions, with implications for hydrogen transport at the Earth's core mantle boundary.[63] However, with the exception of water,[42,65–68] there have been limited in situ experiments on materials which are superionic at high-pressure and high-temperature, and it is possible that future studies will find superionicy in further metal-rich hydrides. Such conditions have become more experimentally accessible in recent years[39,66,68,69] and it may be that the novel modifications to gold chemistry at extreme conditions reported here will be paralleled in other materials.

The gold hydride presented is stable only at high temperature, implying that the transition is entropy driven. It is only experimentally observed under conditions where calculations find the hydrogen to be superionic, and the entropic contribution of the diffusive hydrogen may be required for its stability. Previous attempts to synthesize gold hydride may have succeeded where temperature and pressure were high enough. However, where only quenched samples were subject to structural analysis, as is common in DAC experiments,[25] the gold would have reverted to the *fcc* phase. This might indicate that such unusual chemistry observed only at high pressure and high temperature in the gold–hydrogen system may occur

in other systems, and, given limited studies on metal–hydride chemistry in situ at at high pressure and high temperature, other novel chemical behaviors are waiting to be found in the advancing field of XFEL heating induced chemistry.[36,39,56]

The gold–hydrogen system was previously subject to an ab initio structure search which found no stable phases on the convex hull.[24] Their calculations were performed at zero temperature and do not contradict results reported here which find gold hydride to be stable only at high temperature. Interestingly, they proposed a metastable structure for an Au_2H phase at 200 GPa, but with *Cm* symmetry which appears unrelated to the hexagonal structure observed here. Combined with our experimental confirmation of stable Au─H solid hydrides, this structure predicted at higher pressure may point towards richer gold–hydrogen chemistry at even more extreme conditions.

Hcp gold lattices have previously been investigated using theoretical methods[70,71] and reported in gold nanoclusters.[72] Other non-*fcc* lattices are also reported in gold nanoparticles arising from strain effects[73,74]; however, nonhydrostatic strain will be annealed on formation of the *hcp* phase, as the change in powder texture indicates it undergoes recrystallization. As such, the introduction of hydrogen to the lattice is more likely to be the driving factor for the transition from *fcc* to *hcp*. DFT calculations suggest an *fcc* to *hcp* transition in gold at multi-megabar pressures, though studies disagree on the transition pressure and whether there are intermediate closed packed packed phases with different stacking orders.[71] Experimentally, pure gold with an *hcp* structure has been reported when heated at pressures above 240 GPa,[75] though another study found it to remain *fcc* to at least 1065 GPa at ambient temperature.[76]

Conclusion

In conclusion, we report the synthesis of gold hydride above 40 GPa close to the gold melting point using X-ray heating and diffraction in DACs at the European XFEL. The resulting hydride has variable stoichiometry Au_2H_x, with x increasing from close to 0 at 40 GPa to almost 1 by 80 GPa. It has a hexagonal structure with lattice parameters $a = b \sim 2.75$ Å and $c \sim 4.60$ Å at 55 GPa, possibly related to hexagonal Cu_2H, also known at high pressure. On cooling to ambient temperature, the gold hydride decomposes and *fcc* gold with undetectably low dissolved hydrogen is recovered. The failure of previous efforts to observe gold hydride stability likely arises from its dissociation on cooling which highlights unusual chemical interactions at high pressure and high temperature, which remain poorly explored. The restriction of gold hydride to high temperature conditions implies that its formation is entropy driven, and that an unexplored avenue of chemistry occurs in matter at combined high-pressure and high-temperature conditions. Accompanying DFT-MD simulations have been used to constrain the hydrogen content in the experiments by establishing a molar volume of hydrogen in Au_2H_x. They further reveal hydrogen to be superionic. This is the first report of a binary solid in the gold–hydrogen system and offers insight into the gold–hydrogen interaction. The result implies that the assumed inertness of gold does not extend to extreme conditions.

Supporting Information

Experimental details[50,77–99] are presented in the Supporting Information along with supplemental figures showing additional diffraction data, Raman data, lattice parameters and volumes, Voronoi cell topology analysis, and ionic mobility data.

Acknowledgements

The authors acknowledge the support by J. Sztuk-Dambietz for detector calibration. This work was supported by US Department of Energy (DOE) Office of Fusion Energy Sciences FWP100866. The authors acknowledge European XFEL in Schenefeld, Germany, for provision of x-ray free-electron laser beamtime at Scientific Instrument HED (High Energy Density Science) and would like to thank the staff for their assistance. The authors are indebted to the HIBEF user consortium for the provision of instrumentation and staff that enabled this experiment. The authors acknowledge DESY (Hamburg, Germany), a member of the Helmholtz Association HGF, for the provision of experimental facilities. Parts of this research were carried out at PETRA III beamline P02.2 under proposal I-20230718. The authors gratefully acknowledge the computing time made available to them on the high-performance computers emmy and lise at the NHR Centers Göttingen and Berlin. AFG acknowledges support from the National Science Foundation DMR-2200670 CHE-2302437, and Carnegie Science. EE acknowledges financial support from AEThER by the Alfred Sloan Foundation under grant G202114194. The work of KAbraham, MSchulze, GSN, and RR was supported by the Deutsche Forschungsgemeinschaft (DFG) via the Priority Program SPP 2404 DeepDyn with grant number 521548786. YL and AC acknowledge support by DOE, Office of Science, Basic Energy Sciences, Materials Sciences and Engineering Division under Contract No. DE-AC02-76SF00515 (XFEL experimental assistance). This result is part of a project that has received funding from the European Research Council (ERC) under the European Union's Horizon 2020 research and innovation programme (Grant agreement No. 101002868).

Conflict of Interests

The authors declare no conflict of interest.

Data Availability Statement

The data that support the findings of this study are openly available in the European XFEL data portal at https://doi.org/10.22003/XFEL.EU-DATA-005619-00, reference number 5619.

Keywords: Ab initio calculations · Gold · High-pressure chemistry · Hydrides · X-ray diffraction

[1] H. Schmidbaur, H. G. Raubenheimer, L. Dobrzańska, *Chem. Soc. Rev.* **2014**, *43*, 345–380.
[2] H. G. Raubenheimer, H. Schmidbaur, *J. Chem. Educ.* **2014**, *91*, 2024–2036.
[3] G. J. Kubas, R. Ryan, B. Swanson, P. Vergamini, H. Wasserman, *J. Am. Chem. Soc.* **1984**, *106*, 451–452.
[4] E. Y. Tsui, P. Müller, J. P. Sadighi, *Angew. Chem., Int. Ed.* **2008**, *47*, 8937–8940.
[5] L. Rocchigiani, W. T. Klooster, S. J. Coles, D. L. Hughes, P. Hrobárik, M. Bochmann, *Chem. Eur. J.* **2020**, *26*, 8267–8280.
[6] U. Ringström, *Nature* **1963**, *198*, 981.
[7] H.-T. Liu, Y.-L. Wang, X.-G. Xiong, P. D. Dau, Z. A. Piazza, D.-L. Huang, C.-Q. Xu, J. Li, L.-S. Wang, *Chem. Sci.* **2012**, *3*, 3286–3295.
[8] X. Wang, L. Andrews, *Angew. Chem. Int. Ed.* **2003**, *115*, 5359–5364, *Angew. Chem.* **2003**, *115*, 5359–5364.
[9] X. Wang, L. Andrews, L. Manceron, C. Marsden, *J. Phys. Chem. A* **2003**, *107*, 8492–8505.
[10] H. Schmidbaur, S. Cronje, B. Djordjevic, O. Schuster, *Chem. Phys.* **2005**, *311*, 151–161.
[11] H. Schmidbaur, *Angew. Chem. Int. Ed.* **2019**, *58*, 5806–5809.
[12] H. Darmandeh, J. Löffler, N. V. Tzouras, B. Dereli, T. Scherpf, K.-S. Feichtner, S. Vanden Broeck, K. Van Hecke, M. Saab, C. S. Cazin, L. Cavallo, N. Luigi, P. Steven, V. H. Däschlein-Gessner, *Angew. Chem. Int. Ed.* **2021**, *60*, 21014–21024.
[13] M. Rigoulet, S. Massou, E. D. Sosa Carrizo, S. Mallet-Ladeira, A. Amgoune, K. Miqueu, D. Bourissou, *Proc. Natl. Acad. Sci.* **2019**, *116*, 46–51.
[14] N. Dimitratos, G. Vilé, S. Albonetti, F. Cavani, J. Fiorio, N. López, L. M. Rossi, R. Wojcieszak, *Nat. Rev. Chem.* **2024**, *8*, 195–210.
[15] S. Takano, H. Hirai, S. Muramatsu, T. Tsukuda, *J. Am. Chem. Soc.* **2018**, *140*, 8380–8383.
[16] S.-F. Yuan, J.-J. Li, Z.-J. Guan, Z. Lei, Q.-M. Wang, *Chem. Commun.* **2020**, *56*, 7037–7040.
[17] T. Scheler, M. Marqués, Z. Konôpková, C. L. Guillaume, R. T. Howie, E. Gregoryanz, *Phys. Rev. Lett.* **2013**, *111*, 215503.
[18] T. Matsuoka, M. Hishida, K. Kuno, N. Hirao, Y. Ohishi, S. Sasaki, K. Takahama, K. Shimizu, *Phys. Rev. B* **2019**, *99*, 144511.
[19] A. Aslandukova, A. Aslandukov, D. Laniel, S. Khandarkhaeva, G. Steinle-Neumann, T. Fedotenko, S. V. Ovsyannikov, Y. Yin, F. I. Akbar, K. Glazyrin, M. Bykov, M. Hanfland, C. Giacobbe, E. L. Bright, G. Garbarino, Z. Jia, N. Dubrovinskaia, L. Dubrovinsky, *Phys. Rev. B* **2023**, *107*, 014103.
[20] V. V. Struzhkin, D. Y. Kim, E. Stavrou, T. Muramatsu, H.-k. Mao, C. J. Pickard, R. J. Needs, V. B. Prakapenka, A. F. Goncharov, *Nat. Commun.* **2016**, *7*, 12267.
[21] I. A. Kruglov, D. V. Semenok, H. Song, R. Szcześniak, I. A. Wrona, R. Akashi, M. M. Davari Esfahani, D. Duan, T. Cui, A. G. Kvashnin, A. R. Oganov, *Phys. Rev. B* **2020**, *101*, 024508.
[22] Z. Li, X. He, C. Zhang, X. Wang, S. Zhang, Y. Jia, S. Feng, K. Lu, J. Zhao, J. Zhang, B. S. Min, Y. W. Long, R. C. Yu, L. H. Wang, M. Y. Ye, Z. S. Zhang, V. Prakapenka, S. Chariton, P. A. Ginsberg, J. Bass, S. H. Yuan, H. Z. Liu, C. Q. Jin, *Nat. Commun.* **2022**, *13*, 2863.
[23] F. Schüth, B. Bogdanović, M. Felderhoff, *Chem. Commun.* **2004**, 2249–2258.
[24] M. Rahm, R. Hoffmann, N. Ashcroft, *J. Am. Chem. Soc.* **2017**, *139*, 8740–8751.
[25] C. Donnerer, T. Scheler, E. Gregoryanz, *J. Chem. Phys.* **2013**, *138*.
[26] G. Gao, H. Wang, L. Zhu, Y. Ma, *J. Phys. Chem. C* **2012**, *116*, 1995–2000.
[27] A. F. Goncharov, R. T. Howie, E. Gregoryanz, *Low Temp. Phys.* **2013**, *39*, 402–408.
[28] T. A. Strobel, A. F. Goncharov, C. T. Seagle, Z. Liu, M. Somayazulu, V. V. Struzhkin, R. J. Hemley, *Phys. Rev. B* **2011**, *83*, 144102.
[29] T. Scheler, O. Degtyareva, E. Gregoryanz, *J. Chem. Phys.* **2011**, *135*.
[30] P. Loubeyre, F. Occelli, P. Dumas, *Phys. Rev. B* **2013**, *87*, 134101.
[31] M. Eremets, V. Minkov, P. Kong, A. Drozdov, S. Chariton, V. Prakapenka, *Nat. Commun.* **2023**, *14*, 907.
[32] R. McLellan, *J. Phys. Chem. Solids* **1973**, *34*, 1137–1141.
[33] J. Vetrano, G. Guthrie, H. Kissinger, *Phys. Lett. A* **1967**, *26*, 45–46.
[34] V. Antonov, E. Bokhenkov, B. Dorner, V. Fedotov, G. Grosse, A. Latynin, F. Wagner, R. Wordel, *J. Alloys Compd.* **1998**, *264*, 1–7.
[35] S. S. Lobanov, P.-N. Chen, X.-J. Chen, C.-S. Zha, K. D. Litasov, H.-K. Mao, A. F. Goncharov, *Nat. Commun.* **2013**, *4*, 2446.
[36] M. Frost, R. S. McWilliams, E. Bykova, M. Bykov, R. J. Husband, L. M. Andriambariarijaona, S. Khandarkhaeva, B. Massani, K. Appel, C. Baehtz, O. B. Ball, V. Cerantola, S. Chariton, J. Choi, H. Cynn, M. J. Duff, A. Dwivedi, E. Edmund, G. Fiquet, H. Graafsma, H. Hwang, N. Jaisle, J. Kim, Z. Konôpková, T. Laurus, Y. Lee, H.-P. Liermann, J. D. McHardy, M. I. McMahon, G. Morard, et al., *Nat. Astronomy* **2024**, *8*, 174–181.
[37] D. Kraus, J. Vorberger, N. Hartley, J. Lütgert, M. Rödel, D. Chekrygina, T. Döppner, T. Van Driel, R. Falcone, L. Fletcher, S. Frydrych, E. Galtier, D. O. Gericke, S. H. Glenzer, E. Granados, Y. Inubushi, N. Kamimura, K. Katagiri, M. J. MacDonald, A. J. MacKinnon, T. Matsuoka, K. Miyanishi, E. E. McBride, I. Nam, P. Neumayer, N. Ozaki, A. Pak, A. Ravasio, A. M. Saunders, A. K. Schuster, et al., *Phys. Rev. Res.* **2023**, *5*, L022023.
[38] O. B. Ball, C. Prescher, K. Appel, C. Baehtz, M. Baron, R. Briggs, V. Cerantola, J. Chantel, S. Chariton, A. Coleman, H. Cynn, H. Damker, D. Dattelbaum, L. E. Dresselhaus-Marais, J. H. Eggert, L. Ehm, W. J. Evans, G. Fiquet, M. Frost, K. Glazyrin, A. F. Goncharov, R. J. Husband, H. Hwang, N. Jaisle, Zs. Jenei, J.-Y. Kim, Y. Lee, H.-P. Liermann, J. Mainberger, M. Makita, et al., *J. Appl. Phys.* **2023**, *134*, 055901.
[39] H.-P. Liermann, Z. Konôpková, K. Appel, C. Prescher, A. Schropp, V. Cerantola, R. Husband, J. McHardy, M. McMahon, R. McWilliams, C. M. Pépin, J. Mainberger, M. Roeper, A. Berghäuser, H. Damker, P. Talkovski, M. Foese, N. Kujala, O. B. Ball, M. A. Baron, R. Briggs, M. Bykov, E. Bykova, J. Chantel, A. L. Coleman, H. Cynn, D. Dattelbaum, L. E. Dresselhaus-Marais, J. H. Eggert, L. Ehm, W. J. Evans, G. Fiquet, et al., *J. Synchrotron Radiat.* **2021**, *28*, 688–706.
[40] J. Meza-Galvez, N. Gomez-Perez, A. Marshall, A. Coleman, K. Appel, H. Liermann, M. McMahon, Z. Konôpková, R. McWilliams, *J. Appl. Phys.* **2020**, *127*.
[41] U. Ranieri, L. J. Conway, M.-E. Donnelly, H. Hu, M. Wang, P. Dalladay-Simpson, M. Peña-Alvarez, E. Gregoryanz, A. Hermann, R. T. Howie, *Phys. Rev. Lett.* **2022**, *128*, 215702.
[42] R. Husband, H. Liermann, J. McHardy, R. McWilliams, A. Goncharov, V. Prakapenka, E. Edmund, S. Chariton, Z. Konôpková, C. Strohm, A. Berghäuser, C. Baehtz, J. Chantel, O. B. Ball, L. Andriambariarijaona, M. Bykov, E. Bykova, S. Khandarkhaeva, M. Frost, K. Appel, M. Wilke, M. Makita, G. Fiquet, J. H. Eggert, D. Dattelbaum, H. Cynn, S. Merkel, G. Morard, M. I. McMahon, E. E. McBride, et al., *Nat. Commun.* **2024**, *15*, 8256.
[43] G. Weck, V. Recoules, J.-A. Queyroux, F. Datchi, J. Bouchet, S. Ninet, G. Garbarino, M. Mezouar, P. Loubeyre, *Phys. Rev. B* **2020**, *101*, 014106.

[44] E. A. Lazar, J. Han, D. J. Srolovitz,*Proc. Natl. Acad. Sci.* **2015**, *112*, E5769–E5776.
[45] L. Weinberg, *IEEE Trans. Circuit Theory* **1966**, *13*, 142–148.
[46] P. W. Atkins, J. De Paula, *Atkins' Physical Chemistry*, Oxford University Press, Oxford **2010**.
[47] M. Frost, E. E. McBride, D. Smith, J. S. Smith, S. H. Glenzer, *Adv. Mater. Interfaces* **2023**, *10*, 2202081.
[48] A. Aslandukova, A. Aslandukov, D. Laniel, Y. Yin, F. I. Akbar, M. Bykov, T. Fedotenko, K. Glazyrin, A. Pakhomova, G. Garbarino, S. Khandarkhaeva, S. V. Ovsyannikov, U. Buchenau, R. Ahuja, S. V. Levchenko, G. Steinle-Neumann, S. V. Ovsyannikov, *Sci. Adv.* **2024**, *10*, eadl5416.
[49] M. Frost, D. Smith, E. E. McBride, J. S. Smith, S. H. Glenzer, *J. Appl. Phys.* **2023**, *134*.
[50] J. D. McHardy, C. V. Storm, M. J. Duff, S. G. Macleod, M. I. McMahon, *High Press. Res.* **2023**, *43*, 40–57.
[51] W. Zhang, A. R. Oganov, A. F. Goncharov, Q. Zhu, S. E. Boulfelfel, A. O. Lyakhov, E. Stavrou, M. Somayazulu, V. B. Prakapenka, Z. Konôpková, *Science* **2013**, *342*, 1502–1505.
[52] W. Zhang, A. R. Oganov, Q. Zhu, S. S. Lobanov, E. Stavrou, A. F. Goncharov, *Sci. Rep.* **2016**, *6*, 26265.
[53] M. Bykov, E. Bykova, G. Aprilis, K. Glazyrin, E. Koemets, I. Chuvashova, I. Kupenko, C. McCammon, M. Mezouar, V. Prakapenka, V. Prakapenka, A. I. Chumakov, V. B. Prakapenka, R. J. Husband, J. D. McHardy, M. I. McMahon, S. Khandarkhaeva, S. V. Ovsyannikov, *Nat. Commun.* **2018**, *9*, 2756.
[54] M. Bykov, S. Chariton, E. Bykova, S. Khandarkhaeva, T. Fedotenko, A. V. Ponomareva, J. Tidholm, F. Tasnádi, I. A. Abrikosov, P. Sedmak, A. I. Chumakov, V. B. Prakapenka, V. Cerantola, G. Garbarino, R. J. Husband, J. D. McHardy, M. I. McMahon, *Angew. Chem. Int. Ed.* 2020, *59, 10321–10326;Angew. Chem.***2020**, *132*, 10407–10412.
[55] A. Aslandukov, A. Aslandukova, D. Laniel, I. Koemets, T. Fedotenko, L. Yuan, G. Steinle-Neumann, K. Glazyrin, M. Hanfland, L. Dubrovinsky, N. Dubrovinskaia, *J. Phys. Chem. C* **2021**, *125*, 18077–18084.
[56] E. Siska, G. A. Smith, S. Villa-Cortes, L. J. Conway, R. J. Husband, J. Van Cleave, S. Petitgirard, V. Cerantola, K. Appel, C. Baehtz, V. Bouffetier, *J. Phys. Chem. Lett.* **2024**, *15*, 9912–9919.
[57] M. Miao, Y. Sun, E. Zurek, H. Lin, *Nat. Rev. Chem.* **2020**, *4*, 508–527.
[58] D. V. Semenok, W. Chen, X. Huang, D. Zhou, I. A. Kruglov, A. B. Mazitov, M. Galasso, C. Tantardini, X. Gonze, A. G. Kvashnin, A. R. Oganov, *Adv. Mater.* **2022**, *34*, 2200924.
[59] T. Meier, F. Trybel, G. Criniti, D. Laniel, S. Khandarkhaeva, E. Koemets, T. Fedotenko, K. Glazyrin, M. Hanfland, M. Bykov, G. Steinle-Neumann, *Phys. Rev. B* **2020**, *102*, 165109.
[60] G. J. Irvine, F. Demmel, H. Y. Playford, G. Carins, M. O. Jones, J. T. Irvine, *Chem. Mater.* **2022**, *34*, 9934–9944.
[61] H. Liu, I. I. Naumov, Z. M. Geballe, M. Somayazulu, J. S. Tse, R. J. Hemley, *Phys. Rev. B* **2018**, *98*, 100102.
[62] Y. Zhou, Y. Fu, M. Yang, I. Osmond, R. Jana, T. Nakagawa, O. Moulding, J. Buhot, S. Friedemann, D. Laniel, T. Meier, *Nat. Commun.* **2025**, *16*, 1135.
[63] Y. Zhang, W. Wang, Y. Li, Z. Wu, *Proc. Natl. Acad. Sci.* **2024**, *121*, e2406386121.
[64] M. Caussé, G. Geneste, P. Loubeyre, *Phys. Rev. B* **2023**, *107*, L060301.
[65] M. Millot, F. Coppari, J. R. Rygg, A. Correa Barrios, S. Hamel, D. C. Swift, J. H. Eggert, *Nature* **2019**, *569*, 251–255.
[66] G. Weck, J.-A. Queyroux, S. Ninet, F. Datchi, M. Mezouar, P. Loubeyre, *Phys. Rev. Lett.* **2022**, *128*, 165701.
[67] B. Cheng, M. Bethkenhagen, C. J. Pickard, S. Hamel, *Nat. Phys.* **2021**, *17*, 1228–1232.
[68] V. B. Prakapenka, N. Holtgrewe, S. S. Lobanov, A. F. Goncharov, *Nat. Phys.* **2021**, *17*, 1233–1238.
[69] A. Bommannavar, P. Chow, R. Ferry, R. Hrubiak, F. Humble, C. Kenney-Benson, M. Lv, Y. Meng, C. Park, D. Popov, E. Rod, *Phys. Chem. Miner.* **2022**, *49*, 36.
[70] R. Ahuja, S. Rekhi, B. Johansson, *Phys. Rev. B* **2001**, *63*, 212101.
[71] N. Smirnov, *J. Phys.: Condens. Matter* **2017**, *29*, 105402.
[72] X. Huang, S. Li, Y. Huang, S. Wu, X. Zhou, S. Li, C. L. Gan, F. Boey, C. A. Mirkin, H. Zhang, *Nat. Commun.* **2011**, *2*, 292.
[73] C. Martín-Sánchez, A. Sánchez-Iglesias, J. A. Barreda-Argüeso, J.-P. Itié, P. Chauvigne, L. M. Liz-Marzán, F. Rodríguez, *Nano Lett.* **2025**, *25*, 3588–3596.
[74] C. Martín-Sánchez, A. Sánchez-Iglesias, J. A. Barreda-Argüeso, A. Polian, J.-P. Itié, J. Pérez, P. Mulvaney, L. M. Liz-Marzán, F. Rodríguez, *ACS Nano* **2021**, *15*, 19128–19137.
[75] L. Dubrovinsky, N. Dubrovinskaia, W. A. Crichton, A. S. Mikhaylushkin, S. I. Simak, I. A. Abrikosov, J. S. de Almeida, R. Ahuja, W. Luo, B. Johansson, *Phys. Rev. Lett.* **2007**, *98*, 045503.
[76] N. Dubrovinskaia, L. Dubrovinsky, N. A. Solopova, A. Abakumov, S. Turner, M. Hanfland, E. Bykova, M. Bykov, C. Prescher, V. B. Prakapenka, S. Petitgirard, *Sci. Adv.* **2016**, *2*, e1600341.
[77] M. Frost, C. Curry, S. Glenzer, *J. Instrum.* **2020**, *15*, P05004.
[78] O. Narygina, L. S. Dubrovinsky, C. A. McCammon, A. Kurnosov, I. Y. Kantor, V. B. Prakapenka, N. A. Dubrovinskaia, *Earth Planet. Sci. Lett.* **2011**, *307*, 409–414.
[79] T. S. Sokolova, P. I. Dorogokupets, A. M. Dymshits, B. S. Danilov, K. D. Litasov, *Comput. Geosci.* **2016**, *94*, 162–169.
[80] E. Watkins, R. Huber, C. Childs, A. Salamat, J. Pigott, P. Chow, Y. Xiao, J. Coe, *Sci. Rep.* **2022**, *12*, 631.
[81] A. Dewaele, P. Loubeyre, M. Mezouar, *Phys. Rev. B* **2004**, *70*, 094112.
[82] Y. Akahama, H. Kawamura, *J. Appl. Phys.* **2006**, *100*.
[83] T. Maltezopoulos, F. Dietrich, W. Freund, U. F. Jastrow, A. Koch, J. Laksman, J. Liu, M. Planas, A. A. Sorokin, K. Tiedtke, J. Grünert, *J. Synchrotron Radiat.* **2019**, *26*, 1045–1051.
[84] A. Allahgholi, J. Becker, L. Bianco, A. Delfs, R. Dinapoli, P. Goettlicher, H. Graafsma, D. Greiffenberg, H. Hirsemann, S. Jack, R. Klanner, *J. Instrum.* **2015**, *10*, C01023.
[85] C. Prescher, V. B. Prakapenka, *High Press. Res.* **2015**, *35*, 223–230.
[86] V. Petříček, M. Dušek, L. Palatinus, *Zeitschrift für Kristallographie-Crystalline Materials* **2014**, *229*, 345–380.
[87] A. Dewaele, G. Fiquet, P. Gillet, *Rev. Sci. Instrum.* **1998**, *69*, 2421–2426.
[88] Y. Ye, V. Prakapenka, Y. Meng, S.-H. Shim, *J. Geophys. Res. Solid Earth* **2017**, *122*, 3450–3464.
[89] G. Kresse, J. Furthmüller, *Phys. Rev. B* **1996**, *54*, 11169.
[90] G. Kresse, J. Hafner, *Phys. Rev. B* **1993**, *47*, 558.
[91] P. E. Blöchl, *Phys. Rev. B* **1994**, *50*, 17953.
[92] G. Kresse, D. Joubert, *Phys. Rev. B* **1999**, *59*, 1758.
[93] J. P. Perdew, A. Ruzsinszky, G. I. Csonka, O. A. Vydrov, G. E. Scuseria, L. A. Constantin, X. Zhou, K. Burke, *Phys. Rev. Lett.* **2008**, *100*, 136406.
[94] S. M. Dorfman, V. B. Prakapenka, Y. Meng, T. S. Duffy, *J. Geophys. Res Solid Earth* **2012**, *117*.
[95] K. Takemura, A. Dewaele, *Phys. Rev. B* **2008**, *78*, 104119.
[96] S. Nosé, *J. Chem. Phys.* **1984**, *81*, 511.
[97] W. G. Hoover, *Phys. Rev. A* **1985**, *31*, 1695–1697.
[98] D. Faken, H. Jónsson, *Comput. Mater. Sci.* **1994**, *2*, 279–286.
[99] A. Stukowski, *Modell. Simul. Mater. Sci. Eng.* **2009**, *18*, 015012.

Manuscript received: March 12, 2025
Revised manuscript received: June 23, 2025
Accepted manuscript online: July 03, 2025
Version of record online: August 04, 2025